

Supporting Information for:

Small molecule chelators reveal that iron starvation inhibits late stages of bacterial cytokinesis

Thiago M. A. Santos¹, Matthew G. Lammers¹, Maoquan Zhou¹, Ian L. Sparks¹,
Madhusudan Rajendran¹, Dong Fang², Crystal L. Y. De Jesus¹, Gabriel F. R. Carneiro¹,
Qiang Cui², Douglas B. Weibel^{1,2,3*}

¹*Department of Biochemistry, University of Wisconsin-Madison
440 Henry Mall, Madison, WI 53706, U.S.A.*

²*Department of Chemistry, University of Wisconsin-Madison
1101 University Avenue, Madison, WI 53706, U.S.A.*

³*Department of Biomedical Engineering, University of Wisconsin-Madison
1550 Engineering Drive, Madison, WI 53706, U.S.A.*

*Author to whom correspondence should be addressed:

Douglas B. Weibel

Department of Biochemistry

6424 Biochemical Sciences Building

440 Henry Mall

Phone: +1 (608) 890-1342

Fax: +1 (608) 265-0764

E-mail: douglas.weibel@wisc.edu

Supplementary results and discussion

Other iron chelators arrest bacterial cell division similarly to 1. We expected that cells treated with inhibitory concentrations of iron chelators that are structurally unrelated to **1** would also arrest cell division. We tested this prediction by measuring the growth and morphological changes of *E. coli* cells in medium containing 2× MIC (400 μM) of **2**. *E. coli* cells treated with **2** displayed an identical phenotypic alteration observed in cells treated with **1** (Figures 1b–d). The average cell length of the **2**-treated *E. coli* cell population is significantly higher ($L = 2.7 \pm 0.8 \mu\text{m}$, $n = 2,777$, $P \leq 0.001$) than the average cell length of the DMSO treatment (Figure 1d). **2** also causes cytokinetic arrest in *C. crescentus* cells ~4–6 h after drug treatment. The average length of cells 12 h following treatment with **2** was $4.9 \pm 1.4 \mu\text{m}$ ($n = 747$, $P \leq 0.001$ compared to DMSO control). After 6 h, ~66% of the cells were doublets (i.e., $\geq 4 \mu\text{m}$) and displayed cytokinetic arrest (Figure 1e). Flow cytometric analysis of *C. crescentus* cells treated with **2** for 16 h showed a change in the aspect ratio and area of the cell population when compared to DMSO-treated cells (Figure s1a). Although **2** has been widely used as a metal chelator in bacterial studies¹⁻², we were unable to find reports of its effect on cell morphology and division. Only CoCl_2 , CuSO_4 , FeCl_3 , or FeSO_4 antagonized the bacteriostatic effect of **2** and enabled *E. coli* and *C. crescentus* to grow (Figures s1b and s3d).

To verify whether the division defects we observed in cells treated with **1** or **2** were also evident in cells dosed with other iron chelators, we determined the MIC of several well-characterized or putative chelators against *E. coli* cells (Figure s5a), treated cells with 2× MIC of compound, and analyzed the cell morphology. In general, the compounds we tested recapitulated the division defect observed for cells treated with **1** or **2** (Figures s5b and s6), suggesting that iron chelators block bacterial cell division in a

similar manner. The antagonistic effect of metals was not observed for other common antibiotics that target protein or peptidoglycan biosynthesis (Figure s8).

We reasoned that cells growing in iron-depleted medium—in the absence of small molecule chelators—would also display growth impairment and arrested cell division. To test this hypothesis, we grew *E. coli* in medium treated with Chelex, which is a chelating resin that binds transition metal ions—including copper, cobalt, and iron—with different affinities. *E. coli* grown in Chelex-treated medium reaches ~60% of the cell density of a culture grown in regular medium. Only the addition of FeCl₃ or FeSO₄ restored growth completely in Chelex-treated medium (Figure s7a). These results demonstrate that iron depletion with Chelex is sufficient to partially inhibit growth in the absence of small molecule chelators.

To confirm that iron depletion by Chelex inhibits growth by the same mechanism as **1** and other metal chelators, we imaged *E. coli* cells grown in Chelex-treated medium (Figures s7b and s7c). Compared to cells growing in untreated medium, cells growing in Chelex-treated medium were significantly longer and many cells displayed the characteristic arrest in cytokinesis observed when treated with chelators (Figure s7c); addition of 100 μM iron restored cell morphology and size. These results support the hypothesis that the biological activity of **1** and its role in arresting cell division arise from disrupting iron homeostasis by chelating iron.

Finally, consistent with these observations, we found that a chemical probe of divin—incorporating a photoreactive diazirine group and a reactive azide group⁶—complexed the Cu²⁺ catalyst for click chemistry reactions and inhibited the reaction, supporting our hypothesis that the bacteriostatic activity of divin and its role in inhibiting cytokinesis arises from its function as a metal ion chelator.

Supplementary methods

Chemicals and bacterial strains. Reagents for culture medium were from Fisher Scientific and Sigma-Aldrich. All metals used in the experiments were from Sigma-Aldrich or Alfa Aesar and used without further purification (purity was >97%). Chemicals tested in this study were: 1,10-phenanthroline (Sigma-Aldrich), 1b (5-ethyl-5'-phenyl-3'H-spiro[indoline-3,2'-[1,3,4]thiadiazol]-2-one³) (Sigma-Aldrich), 11c (N'-[(E)-(2-hydroxynaphthalen-1-yl)methylidene]-3-(5-chloro-2-methyl-1H-benzimidazol-1-yl)propanehydrazide⁴), 2,2'-bipyridyl (bipy, 2) (Sigma-Aldrich), actinonin (Adipogen), deferasirox (Selleck Chemicals LCC), deferiprone (Sigma-Aldrich), deferoxamine mesylate salt (Calbiochem), divin (N'-[(E)-(2-hydroxynaphthalen-1-yl)methylidene]-3-(2-methyl-1H-benzimidazol-1-yl)propanehydrazide, 1⁴⁻⁵), D-penicillamine (Alfa Aesar), DTPA (diethylenetriaminepentaacetic acid) (Sigma-Aldrich), EDTA (ethylenediaminetetraacetic acid) (Acros Organics), NIH (2-hydroxyl-naphthylaldehyde benzoyl hydrazone) (Sigma-Aldrich), pyrogallol (Sigma-Aldrich), and TPEN (N,N,N',N'-tetrakis(2-pyridylmethyl)ethylenediamine) (Sigma-Aldrich). Stock solutions of these chemicals were prepared in DMSO or water. Bacterial strains and plasmids used in this study are listed in Table s1.

Genetic methods. Standard procedures were used for genomic and plasmid DNA purification, restriction endonuclease digestion, DNA amplification, gene cloning, and transformation. We used MasterPure DNA Purification Kit (Epicentre) to isolate genomic DNA. Oligonucleotide primers were obtained from IDT and restriction enzymes were from Promega or New England Biolabs. We used Q5 High-Fidelity DNA Polymerase (New England Biolabs) to produce DNA for cloning, and GoTaq DNA polymerase (Promega) for general analytical PCR. Control reactions were always tested

side-by-side. Gene cloning was performed using the In-Fusion HD Cloning Plus kit (Clontech Laboratories). Plasmid constructs were purified using a QIAprep Miniprep Kit (Qiagen) and verified by PCR and sequencing. We used electroporation or chemical methods to transform *E. coli* strains with plasmids. P1 phage transduction was used to transfer selectable genetic markers between *E. coli* strains. When necessary, we removed the cassette FRT-*kan*-FRT using plasmid pCP20⁶. We verified chromosomal deletions and integrations by testing for the presence of antibiotic markers, PCR analysis, and sequencing. Primers used in this study are listed in Table s2.

Minimum inhibitory concentration (MIC) assays. We used the broth microdilution method according to the Clinical and Laboratory Standards Institute (CLSI) standard protocol. Briefly, *E. coli* strains, *C. crescentus* CB15N, and *B. subtilis* 168 were grown overnight for 12 h in M8 minimal medium, PYE broth, and BBM, respectively, at the appropriate temperature with agitation (200 r.p.m.), diluted (1:100) in fresh medium, and grown to mid-exponential phase. *S. pyogenes* ATCC 12344 cultures were grown overnight for 16–18 h at 37°C in BHI broth in a static incubator. The cultures were calibrated to a final concentration of $\sim 10^5$ colony-forming unit (CFU) mL⁻¹ and 100- μ L aliquots of the adjusted cultures were transferred to a 96-well plate. We transferred additional 100- μ L aliquots of the adjusted culture to the top wells, added the drug to be tested and performed 2-fold serial dilutions. We incubated for 16–18 h at 37°C with agitation (200 r.p.m.) for *E. coli* and *B. subtilis* 168, 24 h at 30°C with agitation (200 r.p.m.) for *C. crescentus*, and 16–18 h at 37°C for *S. pyogenes*. The MIC was defined as the lowest concentration of antimicrobial agent that produced no visible growth. We performed the assay in triplicates with, at least, two biological replicates for each

compound and strain combination. Control experiments to verify culture viability and sterility were performed in parallel.

Growth curves. Cultures of *E. coli* BW25113 $\Delta tolC$ were grown overnight in M8 minimal medium for 12 h at 37°C with agitation (200 r.p.m.), diluted (1:100) in fresh medium, incubated at 37°C with agitation (200 r.p.m.), calibrated to an absorbance of 1.0 ($\lambda = 600$ nm), and used as inoculum in the growth curve experiments. To study the time-dependent antagonistic effect of metals on **1**-treated cells, we monitored bacterial growth of *E. coli* cells in M8 minimal medium containing 25 μ M ($2\times$ MIC) of **1** and various concentrations of $\text{CoCl}_2\cdot 6\text{H}_2\text{O}$, $\text{CuSO}_4\cdot 5\text{H}_2\text{O}$, $\text{FeSO}_4\cdot 7\text{H}_2\text{O}$, or $\text{FeCl}_3\cdot 6\text{H}_2\text{O}$. We monitored two different growth conditions. In the first condition, metals were added simultaneously with **1**, cells were incubated at 37°C in a microplate reader, and the absorbance ($\lambda = 600$ nm) was measured every 10 min for 16 h. We performed similar experiments with **2**. In the second condition, **1** was added to the culture, cells were incubated at 37°C in a microplate reader, and the absorbance ($\lambda = 600$ nm) was measured every 10 min for 16 h. Following the 16 h incubation time, we added metals to the culture, incubated cells at 37°C in a microplate reader, and measured the absorbance ($\lambda = 600$ nm) every 10 min for an additional 12–14 h.

Peptidoglycan labeling with fluorescent D-amino acids. *C. crescentus* CB15N cells were grown overnight in PYE broth, diluted (1:100) in 5 mL of fresh PYE broth, and incubated at 30°C with agitation (200 r.p.m.) to an absorbance of 0.1 ($\lambda = 600$ nm). We treated 1 mL aliquots of the cell culture with DMSO, $2\times$ MIC of **1** (25 μ M) or **2** (400 μ M),

and incubated the cells for 6 or 16 h at 30°C with agitation (200 r.p.m.). Following the incubation time, we added 0.5 mM HADA (a fluorescent hydroxycoumarin derivative of D-alanine)⁷ to the cultures and incubated the cells at 30°C with agitation (200 r.p.m.) for 10 min. To remove excess, unincorporated probe, we washed the cells three times with 1 mL of 1× M2 salts at 25°C and resuspended the pellet in 1 mL of 1× M2 salts. We imaged the cells as described above and used Oufti⁸ to measure the spatial localization of HADA incorporation.

Flow cytometry. Cultures of *E. coli* BW25113 $\Delta tolC$ were grown overnight in M8 minimal medium for 12 h at 37°C with agitation (200 r.p.m.), diluted (1:100) in fresh M8 minimal medium, and incubated at 37°C with agitation (200 r.p.m.) to an absorbance of 0.1 ($\lambda = 600$ nm). Cultures of *C. crescentus* CB15N were grown in PYE broth for 24 h at 30°C with agitation (200 r.p.m.), diluted (1:100) in fresh PYE medium, and incubated at 37°C with agitation (200 r.p.m.) to an absorbance of 0.1 ($\lambda = 600$ nm). An aliquot of 6 mL of each calibrated culture was treated with DMSO, deionized water, or 2× MIC of test compounds. We incubated the cultures for 16 h at 37°C or 30°C with agitation (200 r.p.m.), harvested the cells by centrifugation for 5 min at 10,000 g at 25°C, and resuspended the pellet in 4 mL of 1× PBS. We labeled an aliquot of 1 mL of the cell suspension with FM4-64 (Thermo Fisher Scientific), PicoGreen (Thermo Fisher Scientific), or both dyes. We incubated the cell suspensions at 25°C in the dark for 30 min, harvested the cells by centrifugation for 5 min at 10,000 g at 25°C, discarded the supernatant, and resuspended the cell pellets in 1 mL of 1× PBS. Cells were kept on ice in the dark.

Cells in suspension were automatically imaged in flow using the ImageStream

MkII Imaging Flow Cytometer (Amnis/EMD Millipore). We acquired images simultaneously in four channels [bright field (transmitted light), dark field (side scatter), the 2 channels of fluorescence corresponding to FM4-64 ($\lambda_{\text{ex}} = 515 \text{ nm}$, $\lambda_{\text{em}} = 640 \text{ nm}$) and Picogreen ($\lambda_{\text{ex}} = 480 \text{ nm}$, $\lambda_{\text{em}} = 530 \text{ nm}$] using a 60 \times objective (Olympus, UPlanApo, 0.9 numeric aperture, $0.3 \times 0.3 \mu\text{m}$ pixel size, $40 \times 170 \mu\text{m}$ field of view, 600 cell/sec imaging rate). We ran single color controls for FM4-64 and Picogreen to correct for spectral overlap across channels. A compensation matrix was derived using the single-color controls acquired under the same experimental conditions as the treatments. We used IDEAS (EMD Millipore/Merck) to analyze the cell size distribution and defined the gates based on the bright field and fluorescent images of each event. For our analysis, we used a gating strategy that favored events containing single cell.

Construction and monitoring of iron-responsive biosensors. We constructed transcriptional fusions of green fluorescent protein (GFP) to two Fur-regulated promoters of *E. coli* in the low-copy-number plasmid pUA66. The vector pUA66 used for construction of these iron-responsive biosensors contains the promoter-less reporter gene *gfp* mutant 2 derivative (*gfpmut2*), which encodes a variant of the green fluorescent protein GFP. Briefly, we amplified the promoter region containing the Fur-binding site (Fur box) of the genes *fepA* and *yncE* from *E. coli* and cloned the fragments upstream of the *gfpmut2* gene. We transformed *E. coli* BW25113 ΔtolC and *E. coli* BW25113 $\Delta\text{tolC} \Delta\text{fur}$ with the plasmids pUA66 (empty vector), pUA66- $P_{fepA}::gfpmut2$, or pUA66- $P_{yncE}::gfpmut2$. To monitor the iron-starvation response in *E. coli* BW25113 ΔtolC and *E. coli* BW25113 $\Delta\text{tolC} \Delta\text{fur}$, cultures were grown overnight in M8 minimal medium for 12 h at 37°C with agitation (200 r.p.m.), diluted (1:100) in fresh M8 minimal medium, and incubated at

37°C with agitation (200 r.p.m.) to an absorbance of 0.4–0.5 ($\lambda = 600$ nm). Calibrated cultures were diluted (1:10,000) ($\sim 10^5$ CFU mL⁻¹) in fresh M8 minimal medium and 200 μ L of the cell suspension was treated with DMSO, 0.5 \times MIC of **1** (6.25 μ M) or **2** (100 μ M), or 100 μ M of FeSO₄. We performed the experiment in a 96-well plate at 37°C and measured the absorbance ($\lambda = 600$ nm) and the GFP fluorescence intensity ($\lambda_{\text{ex}} = 475$ nm, $\lambda_{\text{em}} = 509$ nm) of the cell suspensions every 20 min for 20 h in a Tecan Infinite M200Pro microplate reader (Tecan). Control experiments to verify culture viability and metal toxicity were performed in parallel. We analyzed the iron-starvation response in each treatment as a ratio of the GFP fluorescence intensity to the absorbance when the cells cultures reached an absorbance of 0.18 ($\lambda = 600$ nm).

Molecular modeling and binding affinity determinations. We computed the binding affinity of a hydrated metal ion to metal chelators (two copies of **1** or three copies of **2**) using the approach used in previous studies⁹⁻¹⁰. The structures of the relevant molecules were optimized using density functional theory [B3LYP¹¹⁻¹²] with the LANL2DZ effective core potential/basis set¹³ for the metal and 6-31G(d)¹⁴ on the other atoms. Energetics was further improved with single point calculations with the larger 6-311++G(2d,2p)¹⁵ basis set on the main group elements. Enthalpic and entropic contributions were estimated with vibrational frequency calculations and the rigid-rotor-harmonic-oscillator approximations under the condition of 300 K and 1 atm. Solvation free energies were calculated with the SMD solvation model¹⁶. All calculations are performed using Gaussian 09¹⁷.

Precursor incorporation studies. Cultures of *E. coli* BW25113 Δ *tolC* and *B. subtilis* 168

were grown overnight for 16–20 h at 37°C with agitation (200 r.p.m.), diluted (1:10) in fresh medium, and incubated at 37°C with agitation (200 r.p.m.) to an absorbance of 0.1 ($\lambda = 600$ nm). An aliquot of 1 mL of cell suspension was labeled with 0.5 μ Ci of [6-³H]glucosamine D-hydrochloride (American Radiolabeled Chemicals) (peptidoglycan biosynthesis), [methyl-³H]thymidine (Moravek Biochemicals) (DNA biosynthesis), [5,6-³H]uridine (Moravek Biochemicals) (RNA biosynthesis), or [4,5-³H]L-leucine (Moravek Biochemicals) (protein biosynthesis). After 1 min, we treated the labeled cultures with DMSO, 0.5 \times or 2 \times MIC of **1** or **2**. Vancomycin (2 \times MIC, 400/0.39 μ M for *E. coli*/*B. subtilis*), ciprofloxacin (2 \times MIC, 0.05/1.56 μ M), rifampicin (16 \times MIC, 100 μ M, for *E. coli* and 2 \times MIC, 1.56 μ M, for *B. subtilis*), and chloramphenicol (2 \times MIC, 6.25/25 μ M) served as reference antibiotics for inhibition of peptidoglycan, DNA, RNA, or protein biosynthesis, respectively. After 1h following treatment, we transferred 0.2 mL of aliquots into microcentrifuge tubes containing 0.4 mL of ice-cold, 10% trichloroacetic acid (TCA), mixed thoroughly and incubated the samples at 4°C for at least 12 h. We washed the precipitated material with 0.2 mL of a solution of 5% TCA containing 1.5 M NaCl, followed by washing with 0.2 mL of 5% TCA. After the second wash, we solubilized the samples with 0.2 mL of a solution of 0.1% SDS containing 0.1 M NaOH and vortexed. All centrifugation steps were performed at 10,000 *g* for 10 min at 25°C. The solubilized precipitates were transferred into scintillation tubes and thoroughly mixed with 3 mL of Ultima-Flo AP scintillation cocktail (PerkinElmer). Radioactivity was measured in counts per minute using a Tri-Carb 2100TR liquid scintillation analyzer (Packard/PerkinElmer) and the results were expressed as percentage incorporation compared to the DMSO control.

Measurement of ATP levels. Cultures of *E. coli* BW25113 $\Delta tolC$ were grown overnight in M8 minimal medium for 12 h at 37°C with agitation (200 r.p.m.), diluted (1:100) in fresh M8 minimal medium, incubated at 37°C with agitation (200 r.p.m.), calibrated to an absorbance of 0.1 ($\lambda = 600$ nm). An aliquot (200 μ L) of the calibrated culture was treated with DMSO, 0.5 \times or 2 \times MIC of **1**, **2**, or carbonyl cyanide *m*-chlorophenyl hydrazone (CCCP) and incubated for 1 h at 37°C with agitation (200 r.p.m.). Following incubation, we measured the absorbance ($\lambda = 600$ nm) of the cultures, added 100 μ L of BacTiter-Glo (Promega) reagent to 100 μ L of culture, incubated the mixture for 5 min at 25°C in a rotating platform, and measured luminescence using a Tecan Infinite M1000 microplate reader (Tecan). The relative luminescence was expressed as percentage compared to the DMSO control.

Multicopy suppression screen. We selected 79 genes encoding proteins involved in cell division, envelope biogenesis, and iron metabolism from a library of the *E. coli* K-12 derivative (*E. coli* AG1) strains harboring a complete set of operational reading frames cloned in the multicopy plasmid vector pCA24N⁶. We grew cultures overnight in a 96-well plate in M8 minimal medium supplemented with 20 μ g mL⁻¹ chloramphenicol for 12 h at 37°C with agitation (200 r.p.m.), diluted (1:10) in fresh M8 minimal medium supplemented with 20 μ g mL⁻¹ chloramphenicol, and incubated at 37°C with agitation (200 r.p.m.) to an approximate absorbance of 0.2 ($\lambda = 600$ nm). The cultures were treated with 100 μ M IPTG and grown for 3 h at 37°C with agitation (200 r.p.m.). Following induction, we diluted the cultures (1:10) in 200 μ L of fresh M8 minimal medium supplemented with 20 μ g mL⁻¹ chloramphenicol, 100 μ M IPTG, 100 μ M of the efflux

pump inhibitor phenylalanine-arginine beta-naphthylamide (PAβN), and different concentrations of **1** or DMSO. We measured the initial absorbance ($\lambda = 600$ nm) of the cell suspensions, incubated at 37°C with agitation (200 r.p.m.), and measured the absorbance ($\lambda = 600$ nm) after 24 and 48 h following treatment. We reported bacterial growth in each condition as a ratio relative to growth of the correspondent overexpression strain grown in the absence of **1**.

Gene expression analysis. Cultures of *E. coli* BW25113 $\Delta tolC$ were grown overnight in M8 minimal medium for 12 h at 37°C with agitation (200 r.p.m.), diluted (1:20) in fresh M8 minimal medium, incubated for 2 h at 37°C with agitation (200 r.p.m.), and calibrated to an absorbance of 0.2–0.25 ($\lambda = 600$ nm). An aliquot (8 mL) of calibrated cultures was treated with 100 μ M FeSO₄, 2× MIC of **1** (25 μ M) or **2** (400 μ M), and grown for 1 h at 37°C with agitation (200 r.p.m.). We extracted RNA from four biological replicates for each treatment using TRI-Reagent (Zymo Research) and Direct-zol (Zymo Research). Briefly, we harvested the cells, resuspended the pellets in 750 μ L of TRI-Reagent (Zymo Research), incubated the samples for 5 min at 25°C, added 200 μ L of chloroform, and mixed the sample for 15 sec. Following 3 min of incubation at 25°C, we centrifuged the sample for 15 min at 12,000 g at 4°C, collected the upper aqueous phase, and proceed to RNA purification using Direct-zol (Zymo Research). We measured the RNA concentration using a Nanodrop spectrophotometer and verified the RNA integrity by electrophoresis. We treated the samples with HL-dsDNase (ArcticZymes) and performed analytical PCR with the samples to confirm the absence of DNA contamination in the RNA preparations. We only used RNA preparations that did not

generate PCR fragments. ~1,500 ng of RNA was reverse-transcribed using the High Capacity RNA-to-cDNA Kit (Applied Biosystems/Thermo Fisher Scientific) and treated with RNase H (New England Biolabs) according to the manufacturer's instructions. For qRT-PCR, we monitored amplification and measured the amount of amplification products for each sample in triplicate for each biological replicate in a reaction mixture of 10 μ L [1 \times PowerUp SYBR Green Master Mix (Applied Biosystems/Thermo Fisher Scientific), 5 pmol of forward primer, 5 pmol of reverse primer, and ~10 ng of cDNA] using the Applied Biosystems (ABI) 7500 Real-Time PCR system (Applied Biosystems/Thermo Fisher Scientific). Real-time PCR was performed with an initial incubation of 2 min at 50°C, 2 min at 95°C, followed by 40 cycles of 15 s at 95°C, and 1min at 60°C. Relative quantification of gene expression was calculated using the comparative C_T method ($2^{-\Delta\Delta C_T}$ method) and we used the expression of the reference gene *idnT*¹⁸ as an endogenous control for normalization.

Supporting figures and tables

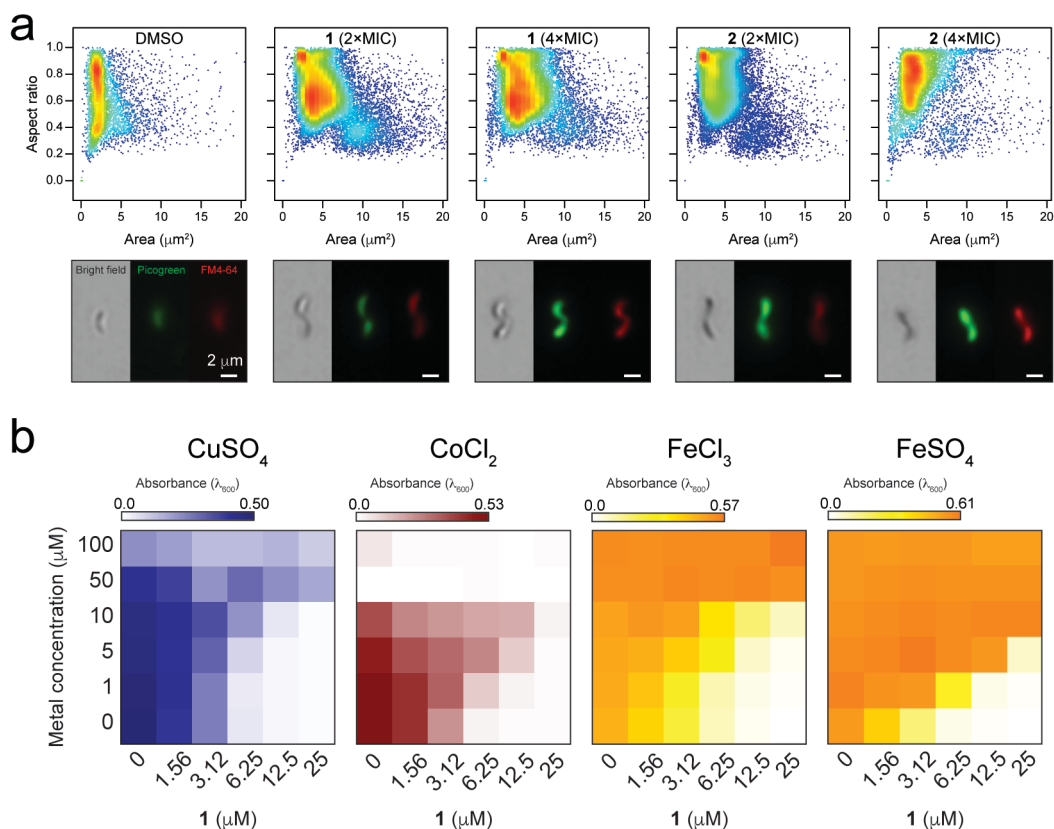


Figure s1. Compounds **1** and **2** inhibit cell division in *C. crescentus*.

(a) Scatter plots displaying the area and aspect ratio of wild-type *C. crescentus* CB15N cells grown for 16 h at 30°C in PYE broth containing DMSO, 2 \times MIC (25 μM) of **1**, 4 \times (50 μM) MIC of **1**, 2 \times MIC (400 μM) of **2**, or 4 \times MIC (800 μM) of **2**. Representative bright field and fluorescence microscopy images of cells from each treatment are displayed below each plot. The images were automatically obtained in flow using the ImageStream MkII Imaging Flow Cytometer. The cell membrane was labeled with FM4-64 (false-colored in red) and DNA was labeled with Picogreen (false-colored in green). Scale bars = 2 μm .

(b) Checkerboard growth assays of the effect of cobalt, copper, and iron in combination with **1** on the growth of wild-type *C. crescentus* CB15N cells. Dark colored squares to white squares represent full growth and complete growth inhibition, respectively. Analyses represent the combination of two independent experiments.

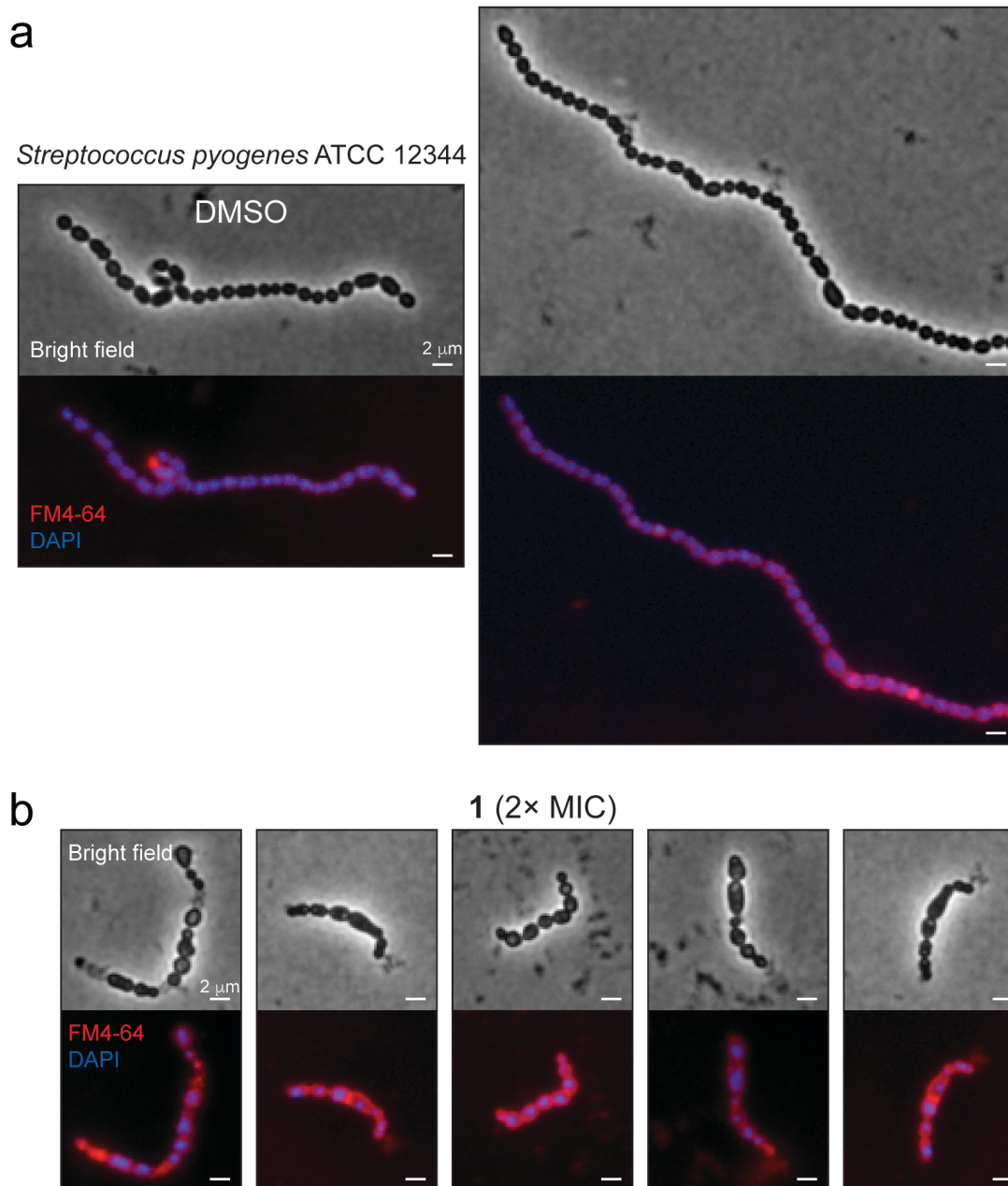


Figure s2. Compound **1** inhibits cell division in *S. pyogenes*.

Representative images of wild-type *S. pyogenes* ATCC 12344 cells grown for 16 h at 37°C in BHI broth containing (a) DMSO or (b) 2 \times MIC of **1** (3.12 μ M). Cell morphology was observed in bright field and fluorescence microscopy images. The cell membrane was

labeled with FM4-64 (false-colored in red) and DNA was labeled with DAPI (false-colored in blue). Scale bars = 2 μm .

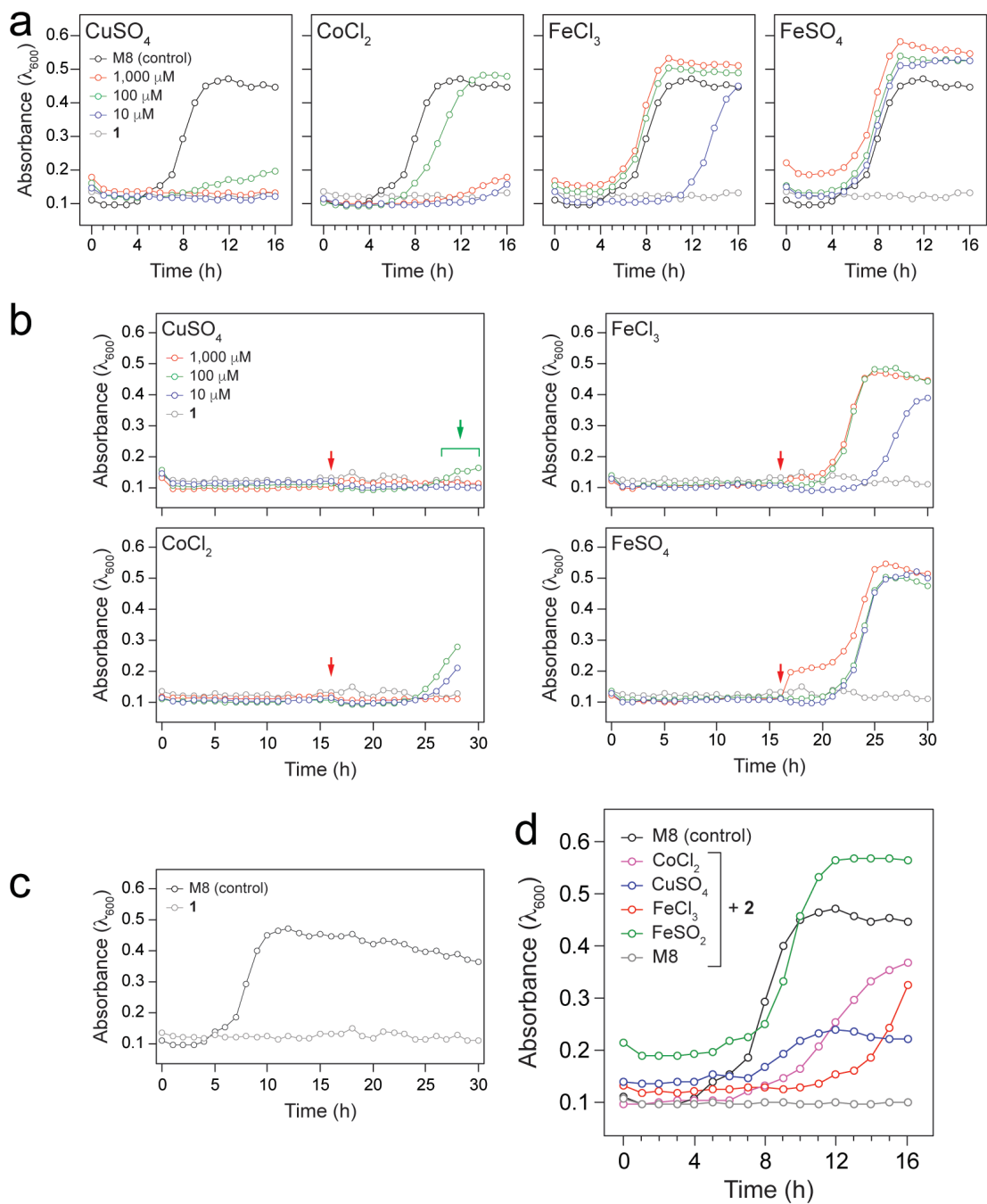


Figure s3. Iron, cobalt, and copper antagonize the biological activity of 1 and 2.

(a) Growth curves of *E. coli* BW25113 $\Delta tolC$ cells in the presence of 2 \times MIC of 1 (25 μ M) and various metals. Control curve (black) shows the growth curve of cells in M8

minimal medium in the presence of DMSO and **1** curve (gray) shows the growth curve of cells in the presence of 2× MIC of **1** without addition of metal.

(b) Growth curves of *E. coli* BW25113 $\Delta tolC$ cells in the presence of 2× MIC of **1** (25 μ M) and various metals. Different concentrations of each metal were added to the cultures at the time point indicated by the red arrow and the additional measurements were taken every hour for about 14 h. **1** curve (gray) shows the growth curve of cells in the presence of 2× MIC of **1** without addition of metal. Green arrow highlights the modest growth of cells in the presence of 2× MIC of **1** and 100 μ M $CuSO_4$.

(c) Growth curve of *E. coli* BW25113 $\Delta tolC$ in M8 minimal medium (black) and in M8 minimal medium containing 2× MIC of **1** (25 μ M) (gray).

(d) Growth curves of *E. coli* BW25113 $\Delta tolC$ in the presence of 1× MIC of **2** (200 μ M) and 100 μ M of various metal ions. M8 control curve (black) shows the growth curve of cells in the presence of DMSO and M8 curve (gray) shows the growth curve of cells in the presence of 1× MIC of **2**.

Growth curves are the average from two independent experiments. Error bars were omitted for clarity.

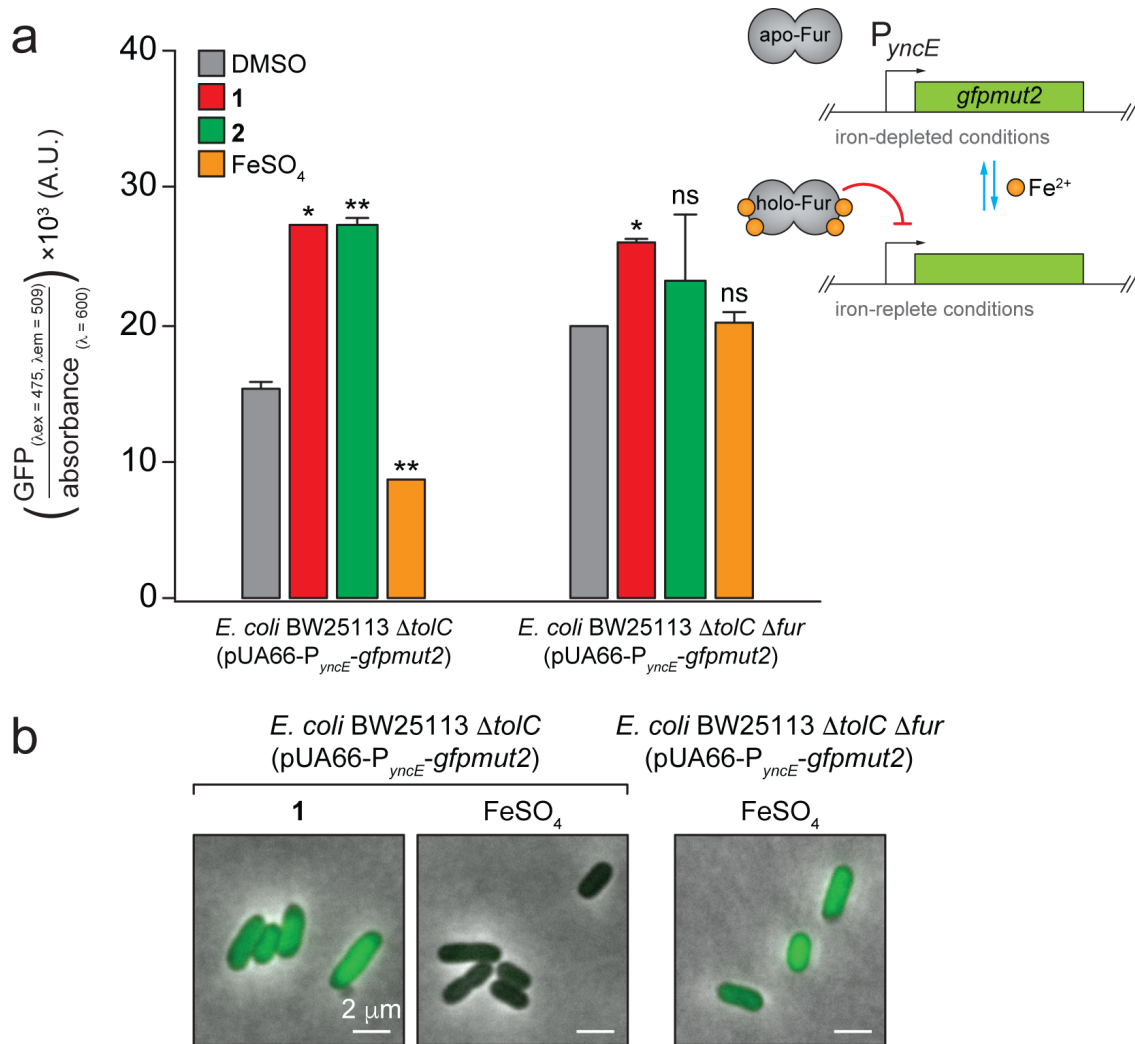


Figure s4. Compound 1 triggers the iron-starvation response in *E. coli*.

(a) Ratio of GFP fluorescence intensity and absorbance of *E. coli* BW25113 $\Delta tolC$ or *E. coli* BW25113 $\Delta tolC \Delta fur$ harboring the plasmid pUA66- P_{yncE} -*gfpmut2* following culturing in M8 minimum medium supplemented with DMSO, 1 (6.25 μ M), 2 (100 μ M), or FeSO₄ (100 μ M). Analyses are the average of two independent experiments. Error bars indicate the standard deviation. *Inset*: A cartoon depicting the classical view of Fur regulation in *E. coli* (summarized in the text). We performed one-sample Student's t-tests to test the

null hypothesis that the GFP fluorescence intensity mean is equal to 100 (the normalized signal for the DMSO control). ns, non-significant; *, $P < 0.05$; **, $P < 0.01$ compared to the DMSO control treatment.

(B) Representative microscopy images of *E. coli* BW25113 $\Delta tolC$ or *E. coli* BW25113 $\Delta tolC \Delta fur$ harboring the plasmid pUA66- P_{yncE} -*gfpmut2* and treated with **1** (6.25 μ M) or FeSO₄ (100 μ M) for 20 h. Scale bars = 2 μ m.

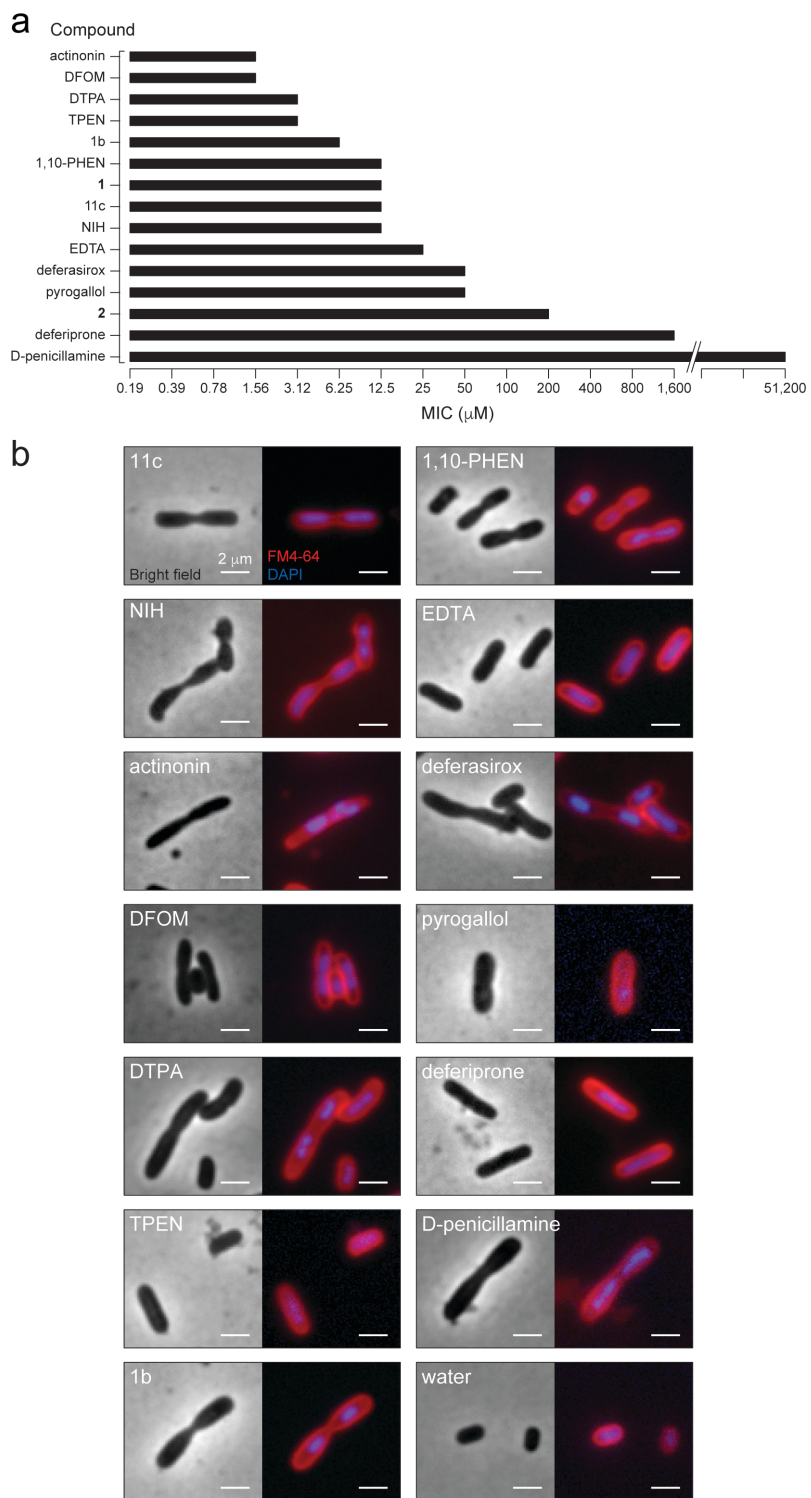


Figure s5. Iron chelators inhibit cell division in *E. coli* by arresting constriction at the division site.

(a) Minimum inhibitory concentration (in μM) of various known and putative iron chelators for *E. coli* BW25113 ΔtolC . Analyses represent a combination of, at least, two independent experiments.

(b) Representative microscopy images of *E. coli* BW25113 ΔtolC cells grown for 16 h at 37°C in M8 minimal medium containing 2× MIC of each compound or solvent indicated. The cell membrane was labeled with FM4-64 (false-colored in red) and DNA was labeled with DAPI (false-colored in blue). Scale bars = 2 μm .

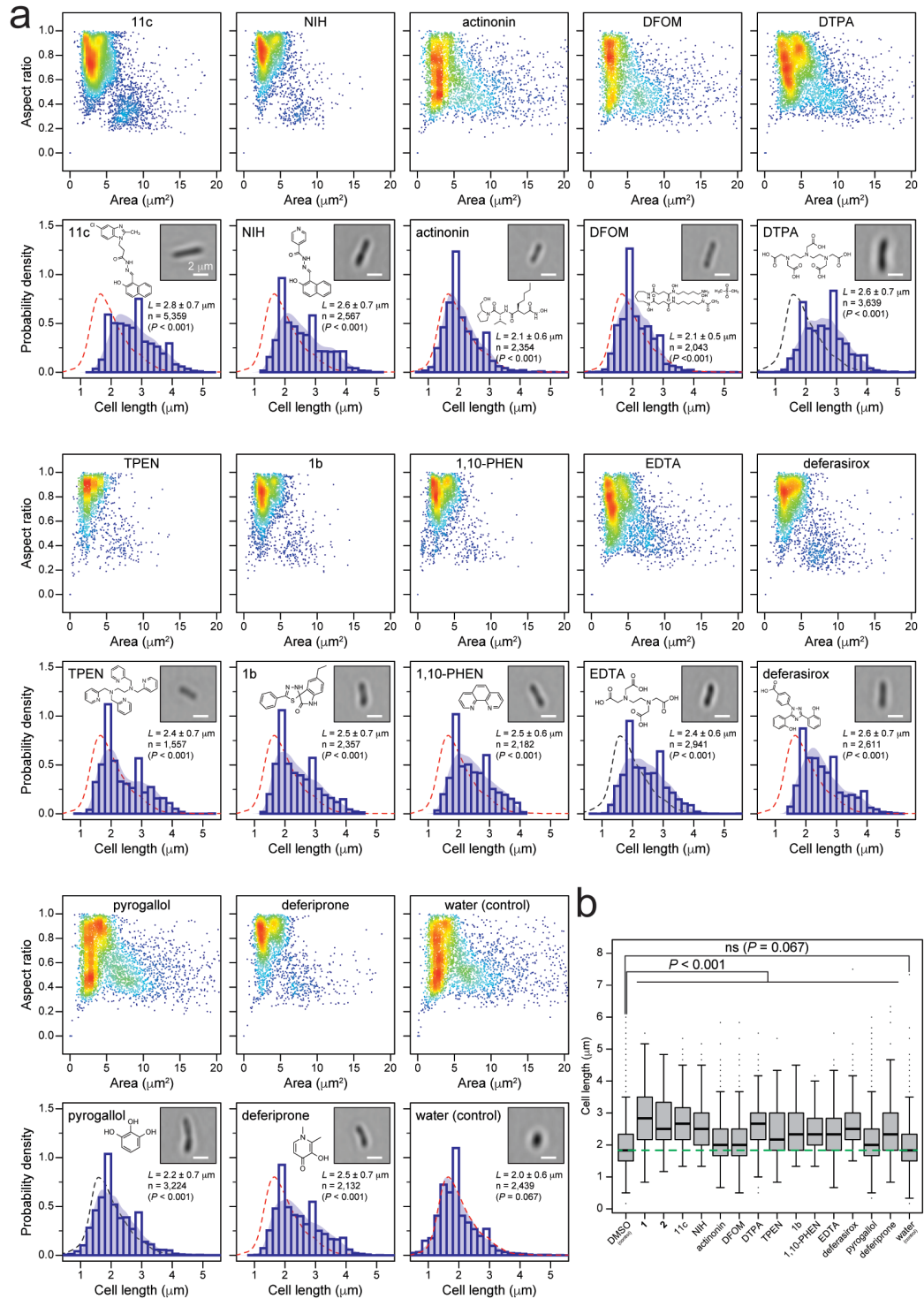


Figure s6. Iron chelators inhibit cell division in *E. coli* by arresting constriction at the division site.

(a) Scatter plots displaying the area and aspect ratio of *E. coli* BW25113 $\Delta tolC$ cells grown for 16 h at 37°C in M8 minimal medium containing 2× MIC of each compound or solvent indicated. Below each scatter plot, we show a probability density histogram of the cell length distribution of events containing single cells. Shaded blue area overlaying the histogram corresponds to the kernel density estimation (KDE) of cell length distribution for the correspondent treatment. Average cell length (L) is given with standard deviations for a total of n cells analyzed. Chemical structure of the compound treatment (except for water) and representative bright field microscopy images of cells from each treatment are displayed in the top part of the histogram. The images were automatically obtained in flow using the ImageStream MkII Imaging Flow Cytometer. Scale bars = 2 μm . Red and black dashed line represents the KDE of the cell length distribution for the DMSO- and water-treated population, respectively, and it was overlaid to facilitate comparison between the treatments and the control group.

(b) Box-and-whisker plots of the cell length of *E. coli* BW25113 $\Delta tolC$ cells grown for 16 h at 37°C in M8 minimal medium containing 2× MIC of each compound or solvent indicated. The extent of the box encompasses the interquartile range (IQR) of the cell length and the black line within each box represents the median. The upper whisker extends to the maximum data value, or 1.5 of the IQR, whichever is the smaller. The lower whisker extends to the minimum data value, or 1.5 of the IQR, whichever is the larger. Outliers are represented as the black dots that do not overlay on top of the box plots. Green dashed line was drawn to facilitate comparison with the median cell length for the DMSO treatment. n.s., non-significant compared to the DMSO control.

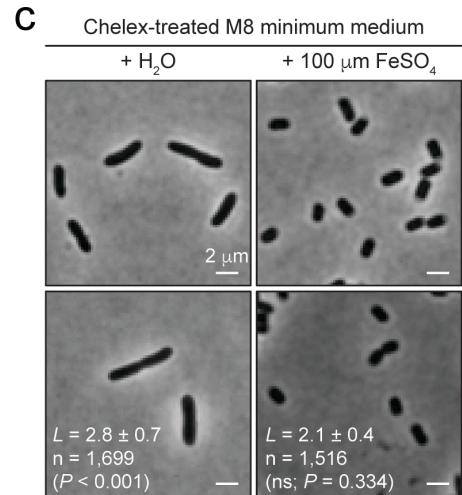
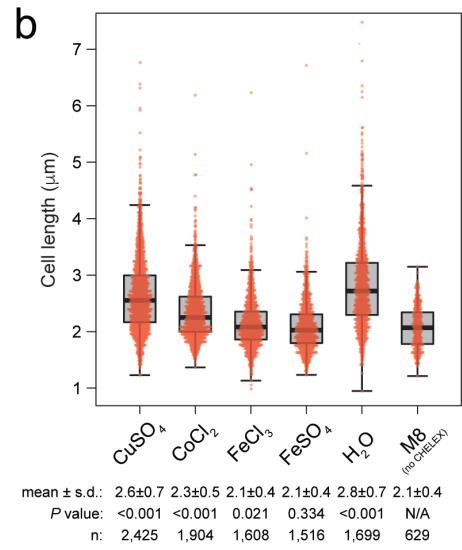
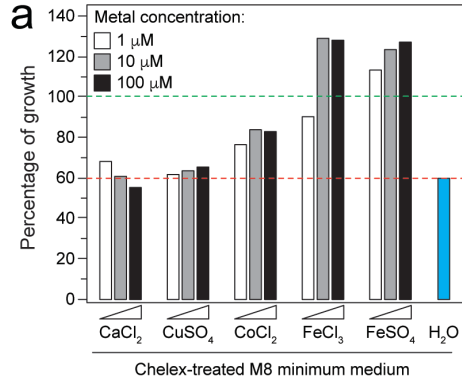


Figure s7. Iron depletion in the absence of a small molecule chelator arrests cell division in *E. coli*.

(a) Growth of *E. coli* BW25113 $\Delta tolC$ in the presence of various metals in Chelex-treated M8 minimal medium without addition of **1**. Bars show the percentage of growth compared to cells growth in regular M8 minimal medium (green dashed line). Red dashed line was drawn to facilitate comparison with the water control. Bars show the percentage of growth compared to cells treated with DMSO and the highest concentration of the respective metal.

(b) Box-and-whisker plots of the cell length of *E. coli* $\Delta tolC$ cells grown for 16 h at 37°C in M8 minimal medium or Chelex-treated M8 minimal medium containing 100 μM or various metals. The extent of the box encompasses the interquartile range (IQR) of the cell length and the black line within each box represents the median. The upper whisker extends to the maximum data value, or 1.5 of the IQR, whichever is the smaller. The lower whisker extends to the minimum data value, or 1.5 of the IQR, whichever is the larger. Overlaid on top of each plot is a bee swarm plot (red circles). Outliers are represented as the red dots that do not overlay on top of the box plots. N/A, not applicable.

(c) Representative images of *E. coli* BW25113 $\Delta tolC$ cells grown for 16 h at 37°C in Chelex-treated M8 minimal medium containing water or 100 μM FeSO_4 . n.s., non-significant compared to the cells grown in regular PYE broth. Scale bars = 2 μm .

In Figures s7b and s7c, average cell length (L) is given with standard deviations for a total of n cells analyzed. Statistical significance for multiple comparisons was determined using a Kruskal-Wallis test with Dunn's post-hoc test.

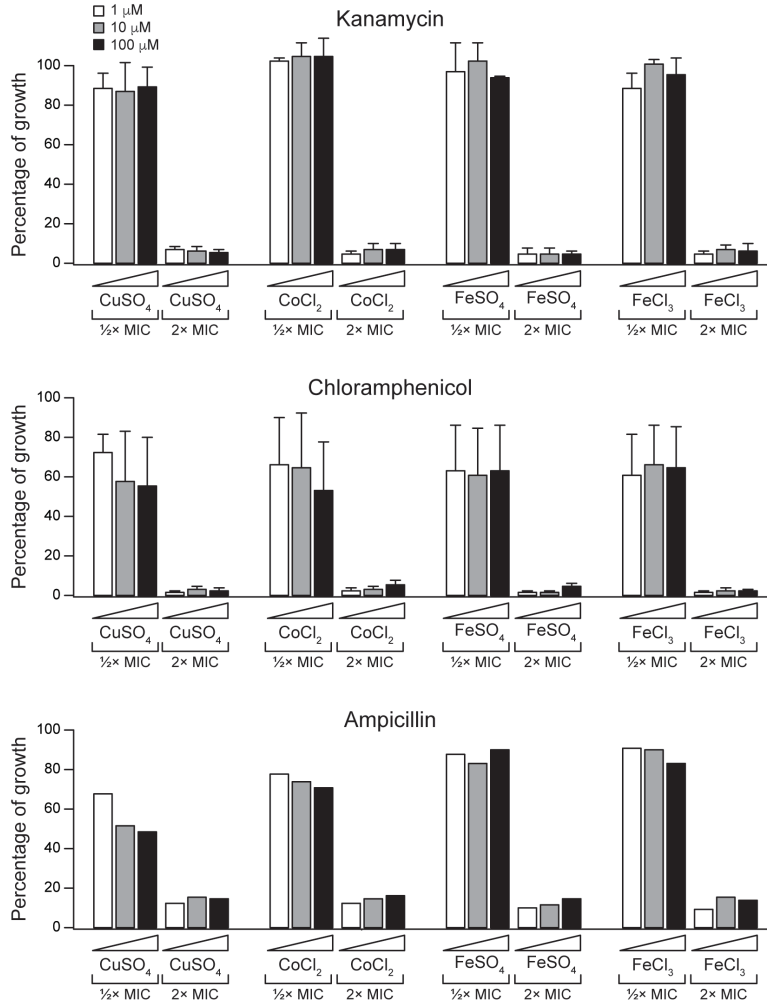


Figure s8. Cobalt, copper, and iron do not antagonize the biological activity of common antibiotics.

Growth of *E. coli* BW25113 $\Delta tolC$ in the presence of 0.5x MIC and 2x MIC of kanamycin, chloramphenicol, or ampicillin in M8 minimal medium supplemented with different concentrations of cobalt, copper, or iron. Growth was calculated as the percentage of growth compared to cells treated with DMSO and the highest concentration of the respective metal. Error bars indicate the standard error of the mean. Except for the treatment with ampicillin, bars are the average from two independent experiments.

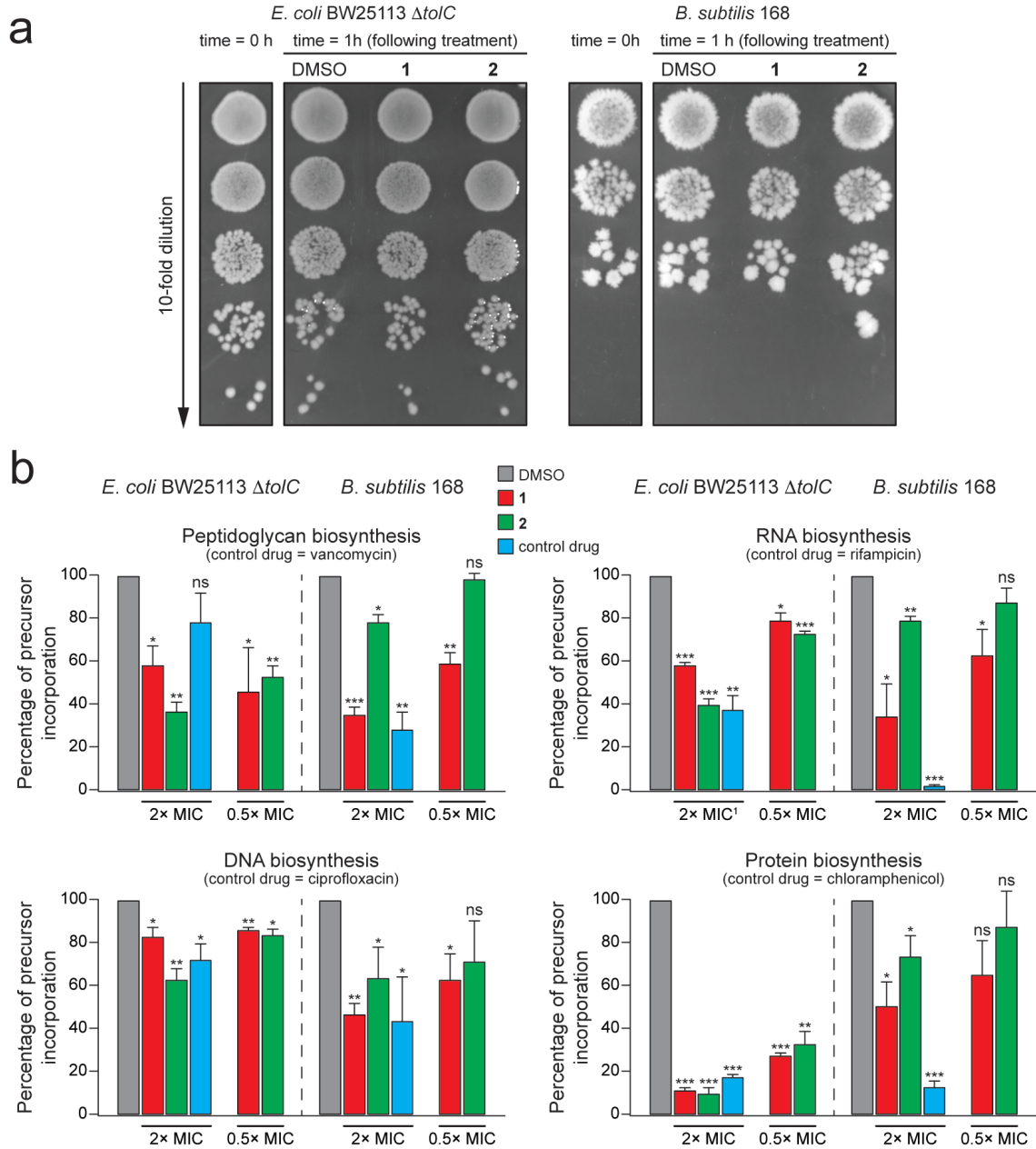


Figure s9. Iron deprivation affects biosynthesis of macromolecules in *E. coli* and *B. subtilis*.

(a) Growth assay of serial dilutions (top to bottom) of *E. coli* BW25113 $\Delta tolC$ and *B. subtilis* 168 before and 1 h after treatment with DMSO, 2× MIC of 1 (25 μ M) or 2 (400 μ M). Aliquots (10 μ L) of 10-fold serial dilutions from each culture were spotted on LB

agar. The plates were incubated at 37°C for 24 h. *Note:* There is no substantial difference in growth following 1 h treatment with DMSO, 2× MIC of **1** or **2**. However, there is a dramatic reduction in biosynthesis of macromolecules following treatment with **1** or **2**.

(b) Biosynthesis of macromolecules in *E. coli* BW25113 $\Delta tolC$ and *B. subtilis* 168 following treatment with **1** or **2**. Incorporation of [6-³H]glucosamine D-hydrochloride into peptidoglycan, [methyl-³H]thymidine into DNA, [5,6-³H]uridine into RNA, or [4,5-³H]L-leucine into protein was determined in cells treated with DMSO, 2× MIC of **1** (25 μM, red) or **2** (400 μM, green). Vancomycin (2× MIC, 400/0.39 μM for *E. coli*/*B. subtilis*), ciprofloxacin (2× MIC, 0.05/1.56 μM), rifampicin (¹16× MIC, 100 μM, for *E. coli* and 2× MIC, 1.56 μM, for *B. subtilis*), and chloramphenicol (2× MIC, 6.25/25 μM) were used as control drugs (blue) and served as reference antibiotics for inhibition of peptidoglycan, DNA, RNA, or protein biosynthesis, respectively. Analyses represent the combination of three independent experiments. Error bars indicate the standard deviation. Results are expressed as percentage of tritium-labeled metabolic precursor incorporation compared to the DMSO control (100% incorporation). To assess differences between the various treatments, we performed one-sample Student's t-tests to test the null hypothesis that the tritium-labeled metabolic precursor incorporation or the ATP level intensity mean is equal to 100 (the normalized incorporation or ATP level for the DMSO control). ns, non-significant; *, $P < 0.05$ **, $P < 0.01$; ***, $P < 0.001$ compared to the DMSO control treatment.

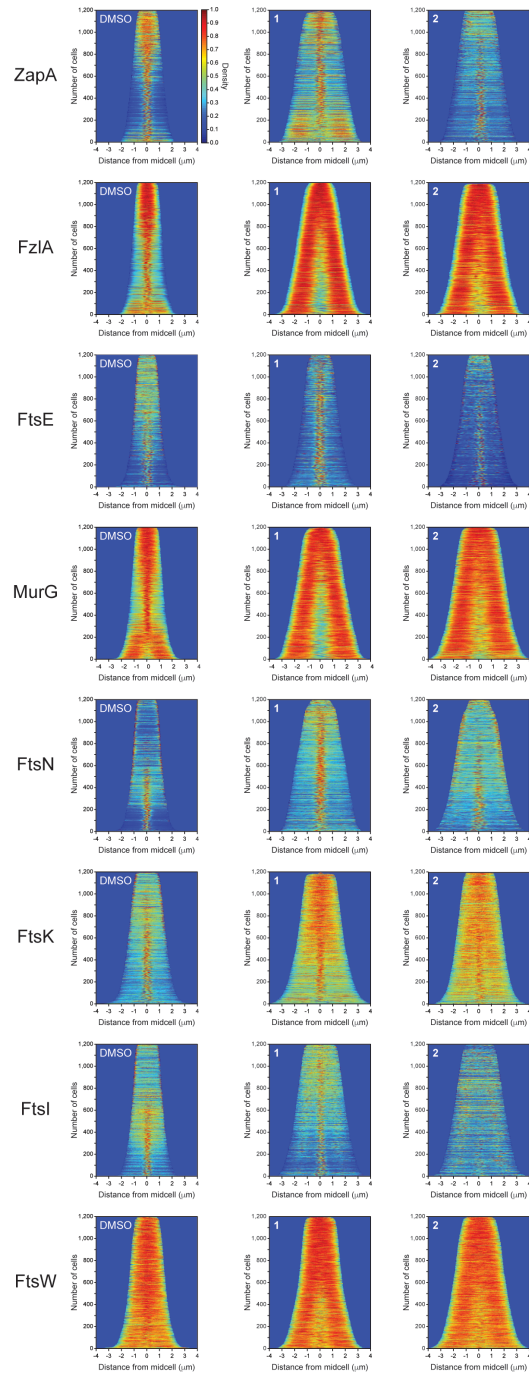


Figure s10. Iron deprivation affects the subcellular localization of cell division proteins. Demographs representing normalized signal profiles of cell division proteins in *C. crescentus* cells arranged by increasing cell length.

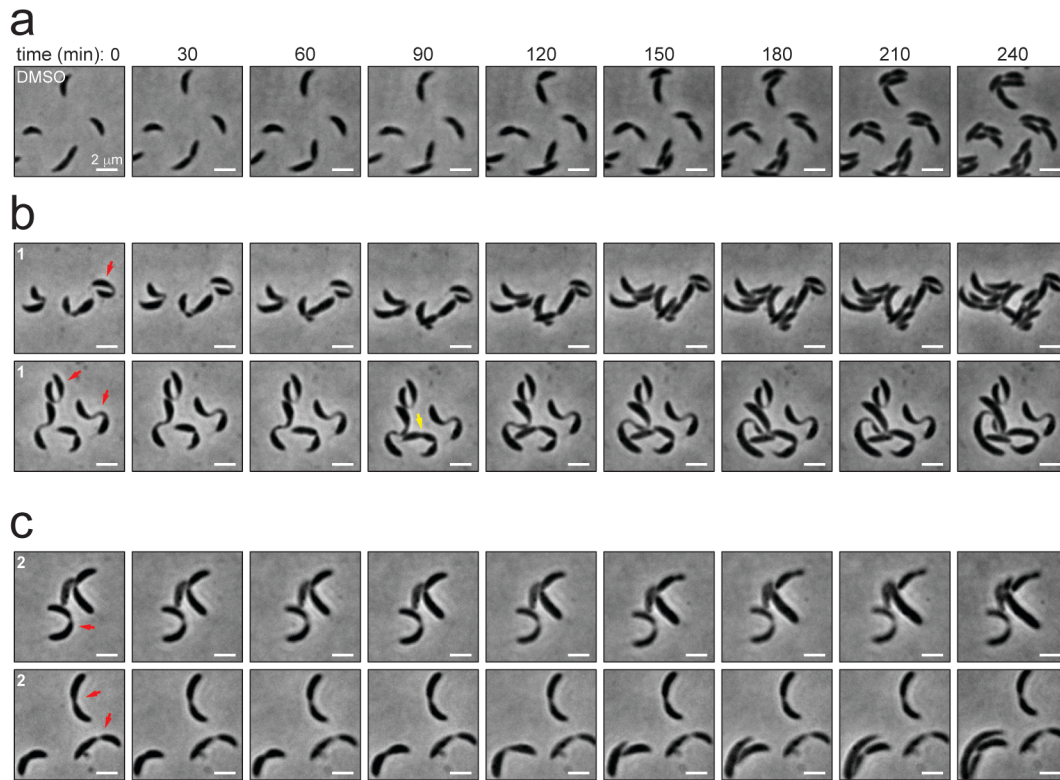


Figure s11. Long-term exposure to iron chelators causes permanent cell division arrest. Bright field microscopy images from time-lapse experiments showing the morphological changes of wild-type *C. crescentus* CB15N cells grown for 4 h at 30°C in PYE agar pads. Prior to each time lapse, cells were grown for 16 h at 30°C in PYE broth containing (a) DMSO, (b) 2× MIC of **1** (25 μM), or (c) 2× MIC of **2** (400 μM). Following this initial treatment, cells were harvested, washed and grown for additional 2 h in fresh PYE broth supplemented with 100 μM of FeSO₄ to allow recovery. Red arrows indicate cells that fail to divide for the duration of the experiment (4 h). Yellow arrow indicates a cell that develops a second division site and completes division at this new site prior to completing division at the primary site. Scale bars = 2 μm.

Table s1. Bacterial strains and plasmids used in this study.

Designation	Genotype or description	Source or reference
Bacterial strain		
<i>Caulobacter crescentus</i> CB15N (or NA1000)	Synchronizable derivative of the wild-type strain CB15	19
<i>C. crescentus</i> EG120	CB15N, <i>ftsI::venus-ftsI</i>	20
<i>C. crescentus</i> EG123	CB15N, <i>ftsW::mCherry-ftsW</i>	20
<i>C. crescentus</i> EG383	CB15N, <i>murG::murG-mCherry</i> , Gm ^K	20
<i>C. crescentus</i> EG384	CB15N, <i>fzIA::mCherry-fzIA</i>	20
<i>C. crescentus</i> EG645	CB15N, <i>zapA::zapA-mCherry</i> , Gm ^K	20
<i>C. crescentus</i> EG652	CB15N, <i>mipZ::mipZ-cerulean ftsE::venus-ftsE</i>	20
<i>C. crescentus</i> EG658	CB15N, <i>ftsK::ftsK-mCherry ftsI::venus-ftsI</i> , Gm ^R	20
<i>C. crescentus</i> MT46	CB15N, <i>ftsN::egfp-ftsN</i>	21
<i>Escherichia coli</i> AG1	<i>recA1 endA1 gyrA96 thi-1 hsdR17 (r K⁻ m K⁺) supE44 relA1</i>	ASKA collection ⁶
<i>E. coli</i> DH5 α	F ⁻ Δ (<i>argF-lac</i>)169 ϕ 80dlacZ(M15) Δ <i>phoA8 glnV44(AS) λ deoR481 rfbC1? gyrA96(NalR) recA1 endA1 thiE1 hsdR17</i>	CGSC#12384 ^a
<i>E. coli</i> BW25113 Δ <i>tolC</i> (<i>E. coli</i> JW5503)	BW25113, Δ <i>tolC732::kan</i> , Km ^R	Keio collection ²²
<i>E. coli</i> BW25113 Δ <i>fur</i> (<i>E. coli</i> JW0669)	BW25113, Δ <i>fur-731::kan</i> , Km ^R	22
<i>E. coli</i> BW25113 Δ <i>tolC::frt</i>	BW25113, Δ <i>tolC732::frt</i> We used the plasmid pCP20 to remove the FRT- <i>kan</i> -FRT cassette from <i>E. coli</i> BW25113 Δ <i>tolC</i> .	This study
<i>E. coli</i> BW25113 Δ <i>tolC</i> Δ <i>fur</i>	BW25113, Δ <i>tolC732::frt</i> , Δ <i>fur-731::kan</i> ^b , Km ^R We used P1 transduction to transfer the FRT- <i>kan</i> -FRT cassette from <i>E. coli</i> BW25113 Δ <i>fur</i> to <i>E. coli</i> BW25113 Δ <i>tolC</i> .	This study
<i>Streptococcus pyogenes</i>	Origin unavailable	ATCC 12344 ^c
Plasmids		
pCP20	Amp ^R , Cm ^R , temperature-conditional replicon expressing a thermal-induced Flp recombinase	23
pUA66 (pUA66- <i>gfpmut2</i>)	Km ^R , the plasmid (pSC101 ori) encodes a promoter-less fast-folding <i>gfpmut2</i> gene as a reporter gene with a strong ribosome binding site, low copy-number	24
pUA66-P _{<i>fcpA</i>} - <i>gfpmut2</i>	Km ^R , this plasmid encodes a fast-folding <i>gfpmut2</i> gene regulated by a P _{<i>fcpA</i>} promoter	This study
pUA66-P _{<i>yncE</i>} - <i>gfpmut2</i>	Km ^R , this plasmid encodes a fast-folding <i>gfpmut2</i> gene regulated by a P _{<i>yncE</i>} promoter	This study

^a CGSC, *Coli* Genetic Stock Center, Yale University.

^b Allele numbers as indicated in the CGSC.

^c ATCC, American Type Culture Collection.

Abbreviation: Amp, ampicillin; Cm, chloramphenicol; Gm, gentamycin; Km, kanamycin; Spec, spectinomycin; Str, streptomycin; R, resistance; frt, indicates the presence of the scar sequence “GAAGTTCCTATTCTCTAGAAAGTATAGGAACTTC” left after removal of the FRT-*kan*-FRT cassette.

Table s2. Primers used in this study.

Primer ^a	Sequence (5'-3') ^b	Reference
<i>Primers for cloning and analytical PCR</i>		
k1	CAGTCATAGCCGAATAGCCT	25
k2	CGGTGCCCTGAATGAACTGC	25
kt	CGGCCACAGTCGATGAATCC	25
entC-F	GCGTTACCTCAAGAGTTGAC	This study
entC-R	GCATGTCGCGTCAGAATGTC	This study
fur-F	CAACATCAGCAGTTTGCC	This study
fur-R	AGACTCATGTCTACGCCG	This study
tolC-F	GTAGCGGCTTCTGCTAGAATCCGCAATAATTTTAC	This study
tolC-R	AGAAGGGGGAAGAATGCGGCAGATAAC	This study
fepA-F-XhoI	TCGTCTTCACCT CGAGT TCGTCATTCAGACGCTGC	This study
fepA-R-BamHI	TAAATCTAGAG GATCCT GTTTTATTCTGCATTTTTGCCACGAAT TGC	This study
yncE-F-XhoI	TCGTCTTCACCT CGAG ACGGGGGAAAGGACAAG	This study
yncE-R-BamHI	TAAATCTAGAG GATC CGACGACTCCCTTTGATGAACCGATA	This study
pUA66-F	GCTTCCCAACCTTACCAGAGGG	This study
pUA66-R	CCACTGACAGAAAATTTGTGCCCA	This study
<i>Primers for qRT-PCR</i>		
entC-F	CAGGCGATGAAAGAGGTAAGT	This study
entC-R	TCAAAGGGAGTTGCGAGATG	This study
fepA-F	CACCTGGTTCCGTAACGATTAT	This study
fepA-R	GCACGTTATCCCAGTATAGAG	This study
ftsQ-F	GGTAGACGCGGAAGGAAATAC	This study
ftsQ-R	GATAGCCCTGCAACACTTCA	This study
ftsW-F	GTAGTGGGTAGCTCGGTAAAG	This study
ftsW-R	GCCTTTACGCACCAGATAGT	This study
ftsZ-F	CGAACGACAAACTGCTGAAAG	This study
ftsZ-R	CATCAAACCCGGACGAGTAAT	This study
idnT-F	CTGTTTAGCGAAGAGGAGATGC	This study
idnT-R	ACAAACGGCGGCGATAGC	This study

^a Oligonucleotide primers were from Integrated DNA Technology, IDT. In general, primer names correspond to the gene that the primer amplifies, the forward (F) primer or the reverse (R) primer of that gene, and the restriction site incorporated into the primer sequence for cloning.

^b The restriction sites used for cloning are in bold.

References

- (1) Seo, S. W.; Kim, D.; Latif, H.; O'Brien, E. J.; Szubin, R.; Palsson, B. O. Deciphering Fur transcriptional regulatory network highlights its complex role beyond iron metabolism in *Escherichia coli*. *Nat Commun* **2014**, *5*, 4910.
- (2) McHugh, J. P.; Rodriguez-Quinones, F.; Abdul-Tehrani, H.; Svistunenko, D. A.; Poole, R. K.; Cooper, C. E.; Andrews, S. C. Global iron-dependent gene regulation in *Escherichia coli*. A new mechanism for iron homeostasis. *J Biol Chem* **2003**, *278*, 29478-29486.
- (3) Falconer, S. B.; Wang, W.; Gehrke, S. S.; Cuneo, J. D.; Britten, J. F.; Wright, G. D.; Brown, E. D. Metal-induced isomerization yields an intracellular chelator that disrupts bacterial iron homeostasis. *Chem Biol* **2014**, *21*, 136-145.
- (4) Zhou, M.; Eun, Y. J.; Guzei, I. A.; Weibel, D. B. Structure-activity studies of divin: An inhibitor of bacterial cell division. *ACS Med Chem Lett* **2013**, *4*, 880-885.
- (5) Eun, Y. J.; Zhou, M.; Kiekebusch, D.; Schlimpert, S.; Trivedi, R. R.; Bakshi, S.; Zhong, Z.; Wahlig, T. A.; Thanbichler, M.; Weibel, D. B. Divin: A small molecule inhibitor of bacterial divisome assembly. *J Am Chem Soc* **2013**, *135*, 9768-9776.
- (6) Kitagawa, M.; Ara, T.; Arifuzzaman, M.; Ioka-Nakamichi, T.; Inamoto, E.; Toyonaga, H.; Mori, H. Complete set of ORF clones of *Escherichia coli* ASKA library (a complete set of *E. coli* K-12 ORF archive): Unique resources for biological research. *DNA Res* **2005**, *12*, 291-299.
- (7) Kuru, E.; Hughes, H. V.; Brown, P. J.; Hall, E.; Tekkam, S.; Cava, F.; de Pedro, M. A.; Brun, Y. V.; VanNieuwenhze, M. S. In Situ probing of newly synthesized peptidoglycan in live bacteria with fluorescent D-amino acids. *Angew Chem Int Ed Engl* **2012**, *51*, 12519-12523.
- (8) Paintdakhi, A.; Parry, B.; Campos, M.; Irnov, I.; Elf, J.; Surovtsev, I.; Jacobs-Wagner, C. Oufiti: An integrated software package for high-accuracy, high-throughput quantitative microscopy analysis. *Mol Microbiol* **2016**, *99*, 767-777.
- (9) Bryantsev, V. S.; Diallo, M. S.; Goddard, W. A., 3rd. Calculation of solvation free energies of charged solutes using mixed cluster/continuum models. *J Phys Chem B* **2008**, *112*, 9709-9719.
- (10) Rao, L.; Cui, Q.; Xu, X. Electronic properties and desolvation penalties of metal ions plus protein electrostatics dictate the metal binding affinity and selectivity in the copper efflux regulator. *J Am Chem Soc* **2010**, *132*, 18092-18102.
- (11) Lee, C.; Yang, W.; Parr, R. G. Development of the Colle-Salvetti correlation-energy formula into a functional of the electron density. *Phys Rev B* **1988**, *37*, 785-789.
- (12) Becke, A. D. Density-functional thermochemistry. III. The role of exact exchange. *J Chem Phys* **1993**, *98*, 5648-5652.
- (13) Hay, P. J.; Wadt, W. R. Ab initio effective core potentials for molecular calculations. Potentials for the transition metal atoms Sc to Hg. *J Chem Phys* **1985**, *82*, 270-283.
- (14) Francl, M. M.; Pietro, W. J.; Hehre, W. J.; Binkley, J. S.; Gordon, M. S.; DeFrees, D. J.; Pople, J. A. Self-consistent molecular orbital methods. XXIII. A polarization-type basis set for second-row elements. *J Chem Phys* **1982**, *77*, 3654-3665.

- (15) Krishnan, R.; Binkley, J. S.; Seeger, R.; Pople, J. A. Self-consistent molecular orbital methods. XX. A basis set for correlated wave functions. *J Chem Phys* **1980**, *72*, 650-654.
- (16) Marenich, A. V.; Cramer, C. J.; Truhlar, D. G. Universal solvation model based on solute electron density and on a continuum model of the solvent defined by the bulk dielectric constant and atomic surface tensions. *J Phys Chem B* **2009**, *113*, 6378-6396.
- (17) Frisch, M. J.; Trucks, G. W.; Schlegel, H. B.; Scuseria, G. E.; Robb, M. A.; Cheeseman, J. R.; Scalmani, G.; Barone, V.; Mennucci, B.; Petersson, G. A.; Nakatsuji, H.; Caricato, M.; Li, X.; Hratchian, H. P.; Izmaylov, A. F.; Bloino, J.; Zheng, G.; Sonnenberg, J. L.; Hada, M.; Ehara, M.; Toyota, K.; Fukuda, R.; Hasegawa, J.; Ishida, M.; Nakajima, T.; Honda, Y.; Kitao, O.; Nakai, H.; Vreven, T.; Montgomery, J. A., Jr.; Peralta, J. E.; Ogliaro, F.; Bearpark, M.; Heyd, J. J.; Brothers, E.; Kudin, K. N.; Staroverov, V. N.; Kobayashi, R.; Normand, J.; Raghavachari, K.; Rendell, A.; Burant, J. C.; Iyengar, S. S.; Tomasi, J.; Cossi, M.; Rega, N.; Millam, J. M.; Klene, M.; Knox, J. E.; Cross, J. B.; Bakken, V.; Adamo, C.; Jaramillo, J.; Gomperts, R.; Stratmann, R. E.; Yazyev, O.; Austin, A. J.; Cammi, R.; Pomelli, C.; Ochterski, J. W.; Martin, R. L.; Morokuma, K.; Zakrzewski, V. G.; Voth, G. A.; Salvador, P.; Dannenberg, J. J.; Dapprich, S.; Daniels, A. D.; Farkas, Ö.; Foresman, J. B.; Ortiz, J. V.; Cioslowski, J.; Fox, D. J. Gaussian 09, Revision E.01. *Gaussian, Inc., Wallingford CT*, **2009**.
- (18) Zhou, K.; Zhou, L.; Lim, Q.; Zou, R.; Stephanopoulos, G.; Too, H. P. Novel reference genes for quantifying transcriptional responses of *Escherichia coli* to protein overexpression by quantitative PCR. *BMC Mol Biol* **2011**, *12*, 18.
- (19) Evinger, M.; Agabian, N. Envelope-associated nucleoid from *Caulobacter crescentus* stalked and swarmer cells. *J Bacteriol* **1977**, *132*, 294-301.
- (20) Goley, E. D.; Yeh, Y. C.; Hong, S. H.; Fero, M. J.; Abeliuk, E.; McAdams, H. H.; Shapiro, L. Assembly of the *Caulobacter* cell division machine. *Mol Microbiol* **2011**, *80*, 1680-1698.
- (21) Moll, A.; Thanbichler, M. FtsN-like proteins are conserved components of the cell division machinery in proteobacteria. *Mol Microbiol* **2009**, *72*, 1037-1053.
- (22) Baba, T.; Ara, T.; Hasegawa, M.; Takai, Y.; Okumura, Y.; Baba, M.; Datsenko, K. A.; Tomita, M.; Wanner, B. L.; Mori, H. Construction of *Escherichia coli* K-12 in-frame, single-gene knockout mutants: The Keio collection. *Mol Syst Biol* **2006**, *2*, 2006 0008.
- (23) Cherepanov, P. P.; Wackernagel, W. Gene disruption in *Escherichia coli*: TcR and KmR cassettes with the option of Flp-catalyzed excision of the antibiotic-resistance determinant. *Gene* **1995**, *158*, 9-14.
- (24) Zaslaver, A.; Bren, A.; Ronen, M.; Itzkovitz, S.; Kikoin, I.; Shavit, S.; Liebermeister, W.; Surette, M. G.; Alon, U. A comprehensive library of fluorescent transcriptional reporters for *Escherichia coli*. *Nat Methods* **2006**, *3*, 623-628.
- (25) Datsenko, K. A.; Wanner, B. L. One-step inactivation of chromosomal genes in *Escherichia coli* K-12 using PCR products. *Proc Natl Acad Sci U S A* **2000**, *97*, 6640-6645.